www.sciencemag.org/content/351/6268/58/suppl/DC1

Supplementary Materials for

Additive manufacturing of polymer-derived ceramics

Zak C. Eckel, Chaoyin Zhou, John H. Martin,
Alan J. Jacobsen, William B. Carter, Tobias A. Schaedler*

*Corresponding author. E-mail: taschaedler@hrl.com

Published 1 January 2016, *Science* **351**, 58 (2016)
DOI: 10.1126/science.aad2688

This PDF file includes:

Materials and Methods
Figs. S1 to S4
Tables S1 to S3
References

Materials

Preceramic Resin System

Several resin systems were explored. To fabricate the structures that were subsequently tested, a UV curable siloxane resin system was formulated by mixing (mercaptopropyl) methylsiloxane (GELEST) with vinylmethoxysiloxane (GELEST) at a 1:1 molar ratio of thiol/vinyl groups, a UV free radical photo initiator at 0.4%, a free radical scavenger as an inhibitor at 0.2 wt% and chemical UV absorber at 0.16 wt%, all tailored to be active at the relevant wave length of UV.

Methods

Additive Manufacturing

The resulting liquid resin was poured into a FormLabs Form1+ SLA printer. Prior to adding the resin, the PDMS layer of the printing bath was coated with a fluorosilicone lubricant to prevent the adhesion of the siloxane to the bath. Printing conditions used were 100µm step sizes with a "flexible resin" setting. The printer uses a UV laser with 405nm wavelength and was operated according to the instructions from the manufacturer Formlabs Inc.

For fabrication of microlattice and honeycomb structures using self-propagating photo-polymer waveguides (SPPW) the same resin system was used without UV absorber using the approach outlined by Jacobsen et al (10). To achieve the curved shape shown in Figure 1C, the "green" polymer structure was manually twisted after extracting it from the resin reservoir and exposed with additional UV light to cure the polymer further in order to maintain that shape. After formation of the pre-ceramic polymer structure, the "green" structure is relatively flexible and can be shaped with little force, for example to a complex curvature. The complex curvature can then be "locked" through a rapid UV post-cure cycle. This is possible because the polymer is not fully crosslinked after the initial UV exposure, if exposure times are selected accordingly. Additional UV exposure increases the level of crosslinking and cures the polymer further increasing its rigidity. A final UV post cure was performed at 125mW/cm^2 for 2 minutes to fully cure the polymer. Once the pre-ceramic polymer structure is post-cured into shape, it can be fired at temperature to form a curved ceramic structure without a high-temperature mandrel and without complex and expensive machining steps (Fig. 1D & S4B). Furthermore, different polymer structures can be joined with small amounts of UV curable resin and the joints can be hardened with a UV exposure. On pyrolysis a continuous ceramic part is formed.

Pyrolysis

The cured preceramic polymer structures were then pyrolyzed in a quartz tube furnace under flowing argon atmosphere. A heating profile of 1^{o}C/min to 1000^{o}C, 60min hold at 1000^{o}C followed by a cooling rate of 3^{o}C/min to room temperature was used. The exhaust gas was run through a bleach/sodium hydroxide scrubber to remove potentially harmful gaseous products formed during pyrolysis. After cool-down, fully ceramic structures were obtained. No additional processing was performed after pyrolysis. A preceramic polymer part and the corresponding pyrolyzed ceramic part is shown in Figure S1.

Mechanical Testing

Compression tests were performed on a servo-electric INSTRON 5960 frame equipped with 500N, 5kN and 50kN load cells (INSTRON). The displacement rate was accurately controlled at 0.5 mm/min for all tests. Samples were bonded to steel facesheets with epoxy adhesive to lock horizontal motion and to offset sample unevenness. Since a considerable amount of epoxy was in the load path, accurate modulus measurements could not be performed in compression. Shear tests were conducted according to ASTM C273, Standard Test Method for Shear Properties of Sandwich Core Materials, with slight deviations in test specimen geometry. Shear plates made of ¼" steel were bonded to the test samples with film adhesive TenCate BF548. Custom fittings were used to mount the shear plates to the load cells and grips. Displacement measurement was performed using a custom fixture with an LVDT (Omega LD400-5) ensuring that only the displacement along the length of the sample is measured. The results of the compression tests are plotted on a materials property chart generated with the CES Selector software from Granta Design Ltd. depicting the yield strength and density of all commercially available materials (Figure S2). It can be seen that the silicon oxycarbide cellular materials are stronger than any other materials available in the density range of 0.1 – 0.8 g/cm^3. Table S2 lists compressive and shear strength of commercially available ceramic foams. Silicon carbide foam is available under the trade name Duocel from ERG Aerospace Corporation and aluminosilicate foam is available from Induceramic Corporation. The properties listed in Table S2 are from datasheets provided by the respective companies.

High Temperature Stability:

11 samples were fabricated and pyrolyzed as described above. The samples were selected to study the silicon oxycarbide microlattice stability at elevated temperatures (full thermal history of samples provided below). Prior beginning the measured mass change of the samples at different temperatures, Samples 1-10 were annealed at 1300C in argon to ensure pyrolysis was taken to completion and the internal structure had stabilized. 1300C was chosen because it was well described in the literature as a threshold temperature before SiC crystallization in SiOC glasses (23). Mass change during the annealing step was approximately 0.3% by weight. Oxidation in air was then studied by heating samples in an open ended tube furnace with porous ceramic thermal blocks at the edges of the hot zone to maintain even heating, but still allow fresh lab air into the hot zone. Heating rates were 5°C/min followed by the desired hold. At the end of the hold the furnace was shut off and the samples were allowed to air cool (generally a few hours to room temperature). After each heating cycle the samples were weighed and photographed (end of cycle indicated as data point in Fig. 4). Samples were divided into batches for each temperature cycle. Data is presented as an average of the batches. Subsequent heat treatments at higher temperatures were performed on some samples as described in detail in Table S3.

Samples 1-10 were fired together in one batch, while sample 11 was fired separately due to the increased size. Initial pyrolysis was completed in a tube furnace under flowing argon as described above. Samples 1 and 2 were subjected to an additional 10 hours at 1300C in Argon to confirm that the material had substantially stabilized. This was

confirmed with subsequent mass change of only 0.05% by weight after 10 hours. Samples 3-10 were also subjected to 10hrs at 1300C in air (average data presented). These showed little to no change (0.15% mass change by weight), and were assumed to be stable with no effect on additional heat treatments. Sample 11 was not annealed at 1300C in argon to confirm that this stabilization step was unnecessary and the microlattice could be used at elevated temperatures directly after 1000C pyrolysis.

The weight yield of microlattice samples after 1 hour exposure in air was 99.98% at 1400°C, 99.05% at 1600°C and 98.79% at 1700°C which compares favorably with the weight yields reported by Xu et al (20): 93.76% at 1400°C, 91.26% at 1600°C and 65.46% at 1700°C. The mass loss is dependent on the surface area, but a surface area is not reported by Xu et al. making a direct comparison impossible. A wide range of oxidation rates has been reported and the mass loss depends strongly on the amount of free carbon. In Figure 4b mass change of other SiOC materials was calculated from parabolic oxidation rate constants for different compositions reported by Modena et al. (24) and Chollon (25). To compare oxidation of different materials in a qualitative way, mass change was extrapolated from reported mass vs. time curves after 1 hour exposure in air.

Material Characterization

To characterize the silicon oxycarbide material in detail, TEM samples were extracted from microlattices using a focused ion beam system. Figure 2 shows a TEM bright field image of a lamella milled out of an as-pyrolyzed silicon oxycarbide microlattice. A homogeneous amorphous microstructure and no porosity is observed. A diffraction pattern taken from the spot indicated by the circle confirms the amorphous nature of the as-pyrolyzed silicon oxycarbide after pyrolysis at 1000°C. Figure 4 shows characterization of a silicon oxycarbide microlattice that had been heat treated for 10 hours at 1300°C followed by 10 hours at 1500°C. A lamella was milled out of a fractured surface of a microlattice strut as indicated by the rectangle in Figure 4C, so that oxide and SiOC base material could be analyzed. Bright field images showed small crystallites of few nanometers in size in both the oxide and SiOC region. High resolution imaging could identify the crystallites as graphite and β-SiC based on the lattice spacing and diffraction pattern. The small size of 5 – 10 μm of the crystals and the high fraction of remaining amorphous matrix indicate that crystallization had just started. The crystallites in the oxide region are even smaller, consistent with the recent formation of this oxide region. Larger crystals are probably present in older oxide layers further from the interface contributing to the cristobalite diffraction pattern recorded by XRD below. Noteworthy were small pores in the SiOC region that were not observed before the heat treatments and presumably developed due to carbon leaving as CO or CO_2 gas. The composition of the oxide region measured by energy-dispersive X-ray spectroscopy (EDS) was 34 at% Si, 2 at% C and 64 at% O. The composition of the SiOC region was 28 at% Si, 31 at% C, 40 at% O, and 1 at% S, within the typical error margin of EDS, when compared to the composition of as –pyrolyzed material measured by Inductively coupled plasma mass spectrometry: 26.7 at% Si, 33.4 at% C, 4.1 at % S and 35.8 at% O.

Powder X-ray diffraction conducted on a crushed silicon oxycarbide microlattice sample after the same heat treatment 1300°C/10h + 1500°C/10h indicated cristobalite

with some amorphous structure (Figure S3), but detected no SiC crystallization, which is consistent with the small size and low volume fraction of the SiC crystals observed in TEM. A few more examples of additively manufactured ceramic parts are shown in Figure S4.

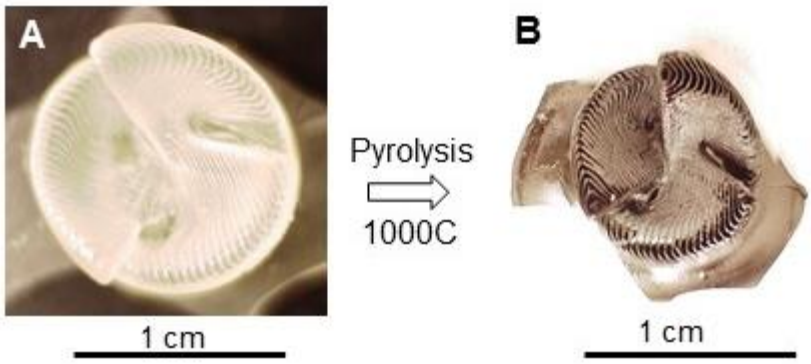

Fig. S1.
3D printed cork screw. (**A**) Preceramic polymer part after 3D printing with SLA printer. (**B**) Ceramic cork screw after pyrolysis.

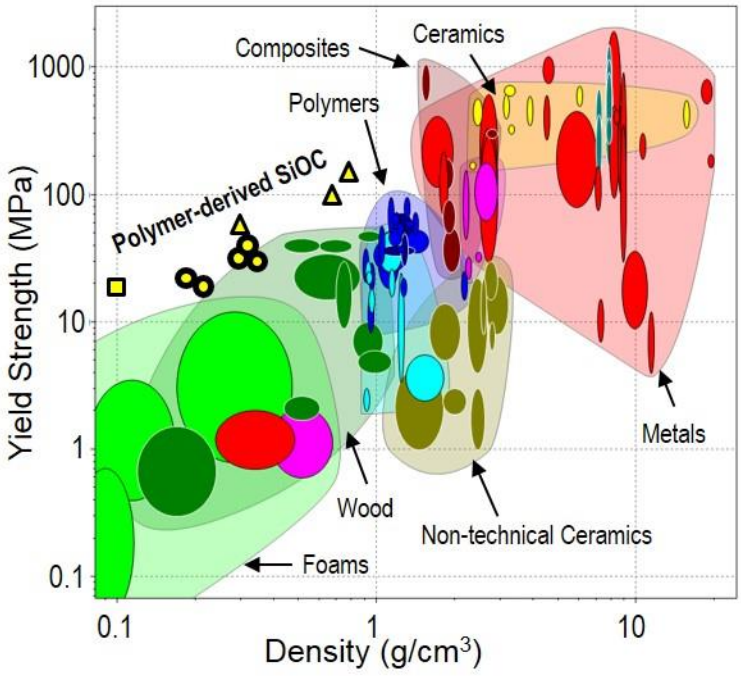

Fig. S2.

Material property chart. The results of the compression tests are plotted on a chart depicting the yield strength and density of all commercially available materials. Square marker: pyramidal truss core, circle marker: microlattice, triangle marker: honeycomb.

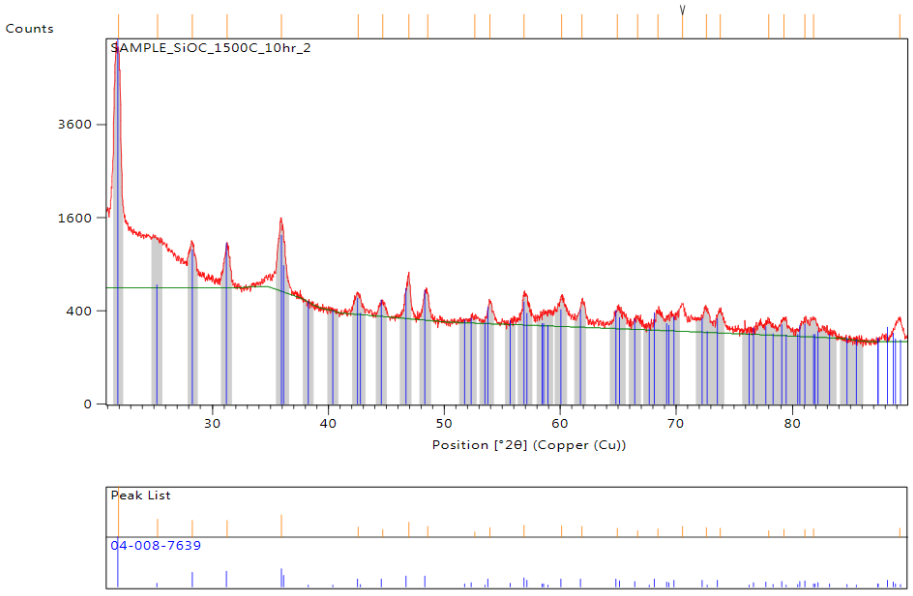

Fig. S3.

X-ray diffraction pattern of a SiOC microlattice crushed into powder after 10 hours at 1500C.

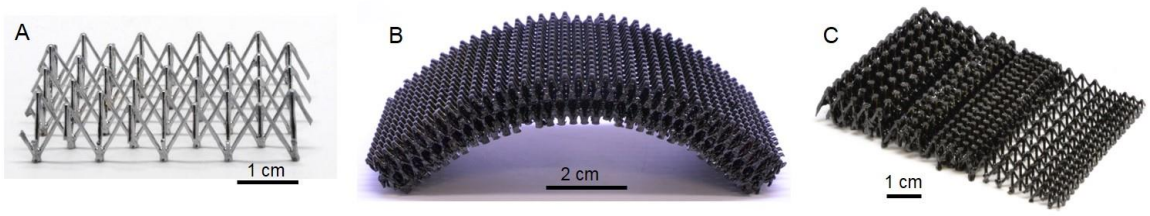

Fig. S4.
Additional examples of ceramic structures fabricated. (**A**) Low density pyramidal truss. (**B**) Curved microlattice. (**C**) Pyramidal truss core with graded density and shape for an airfoil trailing edge.

Table S1.
Mechanical Test Samples

Sample	Architecture	Cell Length L (mm) before pyrolysis	Cell Length L (mm) after pyrolysis	Diameter D (μm) after pyrolysis	Strut Angle θ (°)	Density (g/cm^3)	Relative Density (%)	Compressive Strength (MPa)	Shear Strength (MPa)	Shear Stiffness (MPa)
A	Microlattice	7.2	5.1	0.5	60	0.22	10.7	21		
B	Microlattice	7.2	5.1	0.6	60	0.37	18.1	30		
C	Microlattice	7.2	5.1	0.6	60	0.35	16.9	30.7		
D	Microlattice	7.2	5.1	0.6	60	0.35	17.1	35		
E	Microlattice	7.2	5.1	0.5	60	0.22	10.9	16.6		
F	Pyramidal	14	9.8	0.5	60	0.06	3.1	14.1		
G	Pyramidal	14	9.8	0.5	60	0.06	2.7	9.4		
H	Pyramidal	14	9.8	0.7	60	0.11	5.4	18.9		
I	Honeycomb	10	7.1	1.4	90	0.32	15.4	47.6		
J	Honeycomb	5	3.6	1.0	90	0.70	34.0	98.1		
K	Honeycomb	5	3.6	1.1	90	0.80	39.0	163.3		
L	Microlattice	7.2	5.1	0.5	60	0.22	11.0		4.4	1205
M	Microlattice	7.2	5.1	0.5	60	0.23	11.4		3.7	831
N	Microlattice	7.2	5.1	0.6	60	0.33	16.3		4.2	1576
O	Microlattice	7.2	5.1	0.6	60	0.36	17.3		4.8	939

Table S2.

Properties of Ceramic Foams

Material	Density	Compressive Strength	Shear Strength
	g/cm^3	MPa	MPa
SiC foam Duocel™	0.25	1.38	0.69
AlSiO ceramic foam	0.4	4.23	2.36

Table S3.

Heat Treatment Schedule

Sample #	Pre-Treatment		Heat Treatments						
	Pyrolysis 1000C 1hr in Argon	Anneal 1300C 1hr Argon	1300C 10hr Argon	1300C 10hr Air	Anneal 1400C 1hr Air	1400C 9hr Air (10total)	1500C 10hr Air	1600C 7hr Air	1700C 3hr Air
1	X	X	X					X	
2	X	X	X					X	
3	X	X		X					
4	X	X		X	X	X			
5	X	X		X					
6	X	X		X					
7	X	X		X					
8	X	X		X	X	X			
9	X	X		X	X		X		
10	X	X		X	X		X		
11	X								X

Thermal history proceeds from left to right.

References

1. J. Deckers, J. Vleugels, J.-P. Kruth, Additive manufacturing of ceramics: A review. *J. Ceram. Sci. Technol.* **5**, 245–260 (2014). doi:10.4416/JCST2014-00032

2. N. Travitzky, A. Bonet, B. Dermeik, T. Fey, I. Filbert-Demut, L. Schlier, T. Schlordt, P. Greil, Additive manufacturing of ceramic-based materials. *Adv. Eng. Mater.* **16**, 729–754 (2014). doi:10.1002/adem.201400097

3. A. Zocca, P. Colombo, C. M. Gomes, J. Günster, Additive manufacturing of ceramics: Issues, potentialities and opportunities. *J. Am. Ceram. Soc.* **98**, 1983–2001 (2015). doi:10.1111/jace.13700

4. T. T. Wohlers, T. Caffrey, *Wohlers Report* (Wohlers Associates Inc., Fort Collins, CO, 2013).

5. P. Colombo, G. Mera, R. Riedel, G. D. Sorarù, Polymer-derived ceramics: 40 years of research and innovation in advanced ceramics. *J. Am. Ceram. Soc.* **93**, 1805–1837 (2010). doi:10.1111/j.1551-2916.2010.03876.x

6. S. Martínez-Crespiera, E. Ionescu, M. Schlosser, K. Flittner, G. Mistura, R. Riedel, H. F. Schlaak, Fabrication of silicon oxycarbide-based microcomponents via photolithographic and soft lithography approaches. *Sens. Actuators A Phys.* **169**, 242–249 (2011). doi:10.1016/j.sna.2011.04.041

7. L.-A. Liew, Y. Liu, R. Luo, T. Cross, L. An, V. M. Bright, M. Dunn, J. W. Daily, R. Raj, Fabrication of SiCN MEMS by photopolymerization of pre-ceramic polymers. *Sens. Act. A* **95**, 120–134 (2002). doi:10.1016/S0924-4247(01)00723-3

8. P. Colombo, R. Riedel, G. D. Sorarù, H. J. Kleebe, Eds., *Polymer Derived Ceramics*. (DEStech Publications, Inc., Lancaster, PA, 2010).

9. M. Schulz, M. Börner, J. Göttert, T. Hanemann, J. Haußelt, G. Motz, Cross linking behaviour of preceramic polymers effected by UV- and synchrotron radiation. *Adv. Eng. Mater.* **6**, 676–680 (2004). doi:10.1002/adem.200400082

10. A. J. Jacobsen, W. Barvosa-Carter, S. Nutt, Micro-scale truss structures formed from self-propagating photopolymer waveguides. *Adv. Mater.* **19**, 3892–3896 (2007). doi:10.1002/adma.200700797

11. T. A. Schaedler, A. J. Jacobsen, A. Torrents, A. E. Sorensen, J. Lian, J. R. Greer, L. Valdevit, W. B. Carter, Ultralight metallic microlattices. *Science* **334**, 962–965 (2011). Medline doi:10.1126/science.1211649

12. R. Riedel, A. Kienzle, A. Dressler, L. Ruwisch, J. Bill, F. Aldinger, A silicoboron carbonitride ceramic stable to 2,000°C. *Nature* **382**, 796–798 (1996). doi:10.1038/382796a0

13. M. Zaheer, T. Schmalz, G. Motz, R. Kempe, Polymer derived non-oxide ceramics modified with late transition metals. *Chem. Soc. Rev.* **41**, 5102–5116 (2012). Medline doi:10.1039/c2cs15326b

14. P. Colombo, J. R. Hellmann, D. L. Shelleman, Mechanical properties of silicon oxycarbide ceramic foams. *J. Am. Ceram. Soc.* **84**, 2245–2251 (2001). doi:10.1111/j.1151-2916.2001.tb00996.x

15. L. J. Gibson, M. F. Ashby, *Cellular Solids: Structure and Properties* (Cambridge Univ. Press, Cambridge, UK, 1997).

16. A. J. Jacobsen, W. Barvosa-Carter, S. Nutt, Compression behavior of micro-scale truss structures formed from self-propagating polymer waveguides. *Acta Mater.* **55**, 6724–6733 (2007). doi:10.1016/j.actamat.2007.08.036

17. A. J. Jacobsen, W. Barvosa-Carter, S. Nutt, Shear behavior of polymer micro-scale truss structures formed from self-propagating polymer waveguides. *Acta Mater.* **56**, 2540–2548 (2008). doi:10.1016/j.actamat.2008.01.051

18. T. Varga, A. Navrotsky, J. L. Moats, R. M. Morcos, F. Poli, K. Müller, A. Saha, R. Raj, Thermodynamically stable $Si_xO_yC_z$ polymer-like amorphous ceramics. *J. Am. Ceram. Soc.* **90**, 3213–3219 (2007). doi:10.1111/j.1551-2916.2007.01874.x

19. A. Saha, R. Raj, D. L. Williamson, A model for the nanodomains in polymer-derived SiCO. *J. Am. Ceram. Soc.* **89**, 2188–2195 (2006).

20. T. Xu, Q. Ma, Z. Chen, High-temperature behavior of silicon oxycarbide glasses in air environment. *Ceram. Int.* **37**, 2555–2559 (2011). doi:10.1016/j.ceramint.2011.03.053

21. M. D. Beals, S. Zerfoss, Volume change attending low-to-high inversion of cristobalite. *J. Am. Ceram. Soc.* **27**, 285–292 (1944). doi:10.1111/j.1151-2916.1944.tb14471.x

22. L. Huang, J. Kieffer, Molecular dynamics study of cristobalite silica using a charge transfer three-body potential: Phase transformation and structural disorder. *J. Chem. Phys.* **118**, 1487–1498 (2003). doi:10.1063/1.1529684

23. A. Saha, R. Raj, Crystallization maps for SiCO amorphous ceramics. *J. Am. Ceram. Soc.* **90**, 578–583 (2007). doi:10.1111/j.1551-2916.2006.01423.x

24. S. Modena, G. D. Soraru, Y. Blum, R. Raj, Passive oxidation of an effluent system: The case of polymer-derived SiCO. *J. Am. Ceram. Soc.* **88**, 339–345 (2005). doi:10.1111/j.1551-2916.2005.00043.x

25. G. Chollon, Oxidation behavior of ceramic fibers from the Si-C-N-O system and related sub-systems. *J. Eur. Ceram. Soc.* **20**, 1959–1974 (2000). doi:10.1016/S0955-2219(00)00101-1

26. W. C. Tripp, H. C. Graham, Oxidation of Si_3N_4 in the range 1300°C to 1500°C. *J. Am. Ceram. Soc.* **59**, 399–403 (1976). doi:10.1111/j.1151-2916.1976.tb09505.x

27. E. Opila, S. Levine, J. Lorincz, Oxidation of ZrB_2- and HfB_2-based ultra-high temperature ceramics: Effect of Ta additions. *J. Mater. Sci.* **39**, 5969–5977 (2004). doi:10.1023/B:JMSC.0000041693.32531.d1

28. W. C. Tripp, H. C. Graham, Thermogravimetric study of the oxidation of ZrB_2 in the temperature range of 800°C to 1500°C. *J. Electrochem. Soc.* **118**, 1195–1199 (1971). doi:10.1149/1.2408279

29. J. A. Coppala, M. Srinivasan, K. T. Faber, R. H. Smoak, (The Carborundum Company, USA). High Temperature Properties of Alpha Silicon Carbide, Proceedings of International Symposium on Factors in Densification and Sintering of Oxide and Non-oxide Ceramics, October 3–5, 1978, Hakone, Japan. (Gakujutsu Bunken Fukyu-kai, Tokyo,1979), pp. 400–417.

30. N. M. Geyer, Protection of refractory metals against atmospheric environments. Aeronautical Systems Division Technical Report 61-322, from the published Proceedings for the Materials Symposium, 13–15 September 1961 at Phoenix, Arizona.